

Patchwork: A compact representation for 3D polygonal shapes

Ruichen Zheng¹, Biao Zhang¹, Michael Birsak¹, Mikhail Skopenkov¹, and Peter Wonka¹

King Abdullah University of Science and Technology, Thuwal, 23955, Saudi Arabia
zheng-ruichen@kaust.edu.sa, biao.z@outlook.com, michael.birsak@kaust.edu.sa,
mikhail.skopenkov@gmail.com, pwonka@gmail.com

Abstract. We introduce Patchwork, a new general-purpose shape representation capable of modeling 2D and 3D geometry with a small number of parameters. Patchwork is grounded in a rigorous mathematical framework, providing provable complexity bounds and the ability to approximate arbitrary shapes with arbitrary precision in any dimension. We propose an efficient gradient-based optimization scheme to fit Patchwork representations to 2D and 3D data, along with a novel regularization loss that progressively prunes redundant elements, yielding high compactness after convergence. Our approach offers fast fitting performance, a fraction of the required parameters compared to existing alternatives, and native support for inside-outside classification, making it a versatile and compact representation for geometric learning and reconstruction tasks, with future potential for 3D generation. Our implementation is available at: <https://github.com/Ankbzpx/patchwork-experiment>.

Keywords: 3D representation · Surface reconstruction

1 Introduction

Shape representations are at the core of AI-driven geometry processing. Among the many existing ones, the signed distance function (SDF) and occupancy function proved to be the most efficient. The most direct methods for storing this function are the regular-grid discretization and the Fourier transform. They satisfy the key requirements of generative AI: the parameters of the representations are continuous real numbers, and their quantity is fixed. However, the number of parameters can be large. A more attractive approach, actively developed in recent years, is to use neural networks themselves to represent the function. Our work is devoted to this direction.

While the recent SDF fitting methods leverage neural networks and specialized data structures, such as octrees [32] and hash grids [23], to enhance scalability and expressiveness, we pose the complementary question: What constitutes a more efficient network-friendly shape representation? In seeking the answer, we draw inspiration from Cvxnet [7], which represents the SDF of a convex shape as the soft maximum over a set of linear functions, and composes

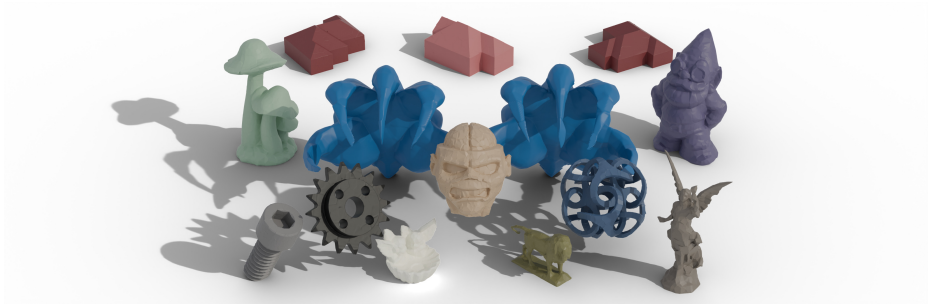


Fig. 1: Our method represents 3D shapes in a very compact and memory-efficient way.

multiple such primitives to model general shapes. While this formulation appears compact, it still introduces inefficiencies: each polyhedron requires multiple sets of coefficients, and the composition of convex parts may overlap, leading to redundancies. To overcome these key limitations, we bring in *Viro’s patchworking* idea from pure mathematics [11]. In patchworks, individual linear functions contribute to the soft maximum with *signs*, resulting in non-convex shapes. Furthermore, we refine this approach by replacing the signs with arbitrary real *weights* and achieving the key principle of a fixed number of real parameters.

However, patchwork optimization is strongly underdetermined, as it implicitly induces the combinatorics of the interface between competing linear functions [29], making it ill-posed for local gradient update. We instead adapt recent advances in deep learning optimization: reparameterization with soft maximum and weight normalization to facilitate gradient updates, regularization through constrained overparameterization that is progressively pruned during optimization, and fully-fused kernels for fast, memory-efficient fitting. Interestingly, our patchwork formulation resembles wide two-layer Multi-Layer Perceptrons (MLPs), yet with proper weight initialization, it has comparable capacity to encode general smooth shapes, matching highly expressive counterparts such as SIREN, while requiring only a fraction of parameters.

In this paper, we develop the theoretical foundation and practical optimization techniques for this new representation and demonstrate that it significantly improves upon competing representations in the low-parameter regime across a wide range of shapes. We envision that our shape representation will be important for compact geometric learning and generative tasks in the future.

Theoretical foundations. Originally, patchwork representation for curves appeared in pure mathematics as a constructive approach to famous *Hilbert’s sixteenth problem*. This problem was stated in the milestone talk “Mathematical Problems” by David Hilbert at the Second International Congress of Mathematicians in 1900. The first part of this problem asked for a possible number and mutual position of components of a curve represented by an algebraic equation of a given degree. This question remains widely open, starting from degree 8. It further decomposes into two sub-tasks: to *construct* an algebraic equation

that represents a curve of given topological type and to *bound* the complexity of algebraic curves of given degree.

Patchworking is an approach to this construction, which traces back to the works by Gudkov [9] from the 1970s and was later formalized and generalized by Viro [36]. See an elementary introduction in [11]. Using this approach, a counterexample to the original Hilbert’s result was constructed (seventy years later), as well as to other famous conjectures in algebraic geometry, and Hilbert’s problem was solved for equations of degree up to 7. Furthermore, it served as a motivation and foundation to *tropical geometry*, which studies piecewise-linear analogs of algebraic curves and surfaces [18]. The underlying formalism has much similarity with neural networks, so it is natural to build a bridge from patchworks to neural shape representations; cf. [4].

The *complexity bounds* for algebraic curves are obtained in *real algebraic geometry* by very different methods [38]. An example is Harnack’s curve theorem, which bounds the number of components of an algebraic curve of given degree. Such results also bound the representation capacity of patchworks. For algebraic surfaces in space, a tight bound is unknown starting from degree 5; see [12].

Contributions. Our contributions are summarized as follows:

- We propose a new shape representation that is expressive and yet compact compared to known alternatives, capable of representing 2D and 3D, smooth and polygonal, convex and non-convex shapes with any precision. It has a simple closed-form expression with a fixed number of real parameters, and built-in connections to neural networks and known mathematical theories.
- We propose geometric initialization and progressive pruning to make fitting our representation viable using gradient descent, yielding high-quality reconstructions comparable to baselines while only requiring a fraction of parameters.
- We implement fully fused kernels that greatly reduce memory consumption.

Organization of the paper. We first discuss related work (Sec. 2), followed by our main concept: patchwork shape representation (Sec. 3). We then introduce practical implementations to make fitting such representations using gradient descent viable (Sec. 4). In Sec. 5 and 6, we discuss the main results and give a concise conclusion. We provide additional theoretical expressiveness and complexity analysis, implementation details, 2D and 3D visual results, direct polygon extraction, and future work in Appendices A–G.

2 Related work

The representation of 3D shapes using neural networks has been explored through various approaches. Early methods focused on modifying the network architecture itself to improve fidelity. For instance, SIREN [30] introduced periodic activation functions for implicit neural representations, while FFN [33] utilized Fourier features to help MLPs learn high-frequency details.

Another line of research pursued acceleration and accuracy by integrating specialized data structures. NGLOD [32] utilized octree data structures, and InstantNGP [23] famously employed multi-resolution hash grids to achieve real-time performance.

More recently, a significant focus has shifted towards compact representations, often with the goal of enabling generative modeling. Works like VecSet [39], M-SDF [37], and efunc [40] have explored compressing shapes into compact representation spaces. Our work shares this objective of achieving a compact and efficient shape representation.

Other methods have approached this problem from different perspectives. Some, like Tulsiani et al. [35], represent shapes using high-level abstractions such as collections of cubes or cylinders. While highly compact, these methods often fail to capture fine-grained geometric details. More relevant to our approach are methods that also utilize hyperplanes to define shapes, such as BSP-Net [5] and CvxNet [7]. However, these methods typically rely on a recursive binary space partitioning scheme, which differs from our method’s use of hyperplanes.

Our approach is directly inspired by the mathematical concept of patchworking [11, 12, 36] and tropical geometry [18]. For applications of tropical geometry for deep learning, see [1, 4, 19, 41].

3 Method

To introduce our main concept, we start with a concise definition in 2D, with a discussion of its visualization and expressive power. Then we generalize it to 3D.

3.1 2D

We represent a curve in the plane as the zero level set of a field $F: \mathbb{R}^2 \rightarrow \mathbb{R}$ of a certain special form.

Definition 1 (See Figs. 2–3). *A 2D patchwork field is a function $\mathbb{R}^2 \rightarrow \mathbb{R}$ of the form*

$$F(x, y) = \frac{1}{\beta} \log \sum_{i=1}^n s_i \exp(\beta (a_i x + b_i y + c_i)), \quad (1)$$

depending on the parameters $n \in \mathbb{Z}_{>0}$ (called width), $\beta \in \mathbb{R}_{>0}$, and $a_i, b_i, c_i, s_i \in \mathbb{R}$, where $i = 1, \dots, n$.

A patchwork is the curve in the plane given by $F(x, y) = 0$.

We also introduce the limiting case $\beta \rightarrow +\infty$ by setting

$$f(x, y) = \max_{i: s_i > 0} \{a_i x + b_i y + c_i\} - \max_{i: s_i < 0} \{a_i x + b_i y + c_i\}, \quad (2)$$

where the first maximum is taken over indices i such that $s_i > 0$ and the second maximum is over i such that $s_i < 0$. The curve given by $f(x, y) = 0$ is also called a patchwork.

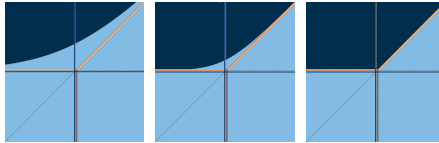


Fig. 2: A patchwork (the boundary between the dark and light areas) for increasing values of β (left and middle) and the limiting case $\beta \rightarrow +\infty$ (right). The design lines (blue), the equality lines (dashed), the candidate intervals (brown/orange), and the active intervals (orange). Just two design lines represent a concave angle.



Fig. 3: Nonconvex (left), disconnected (middle), and non-simply-connected (right) shapes and their approximations by patchworks computed by optimization (right per pair). Each patchwork is the boundary between a dark and a light region. These compact representations have just $n = 12, 37, 55$ design lines (left to right). The candidate intervals (brown/orange) decompose the plane into polygons. The “interior” of the patchwork is roughly the union of the polygons corresponding to the indices i with $s_i < 0$, and the patchwork is roughly the union of active intervals (orange).

Visualization. This construction is visualized as follows; see Fig. 2. Consider the patchwork $f(x, y) = 0$ and let us determine its shape. Introduce the linear function

$$l_i(x, y) := a_i x + b_i y + c_i \quad \text{for each } i = 1, \dots, n. \quad (3)$$

Assume that the functions $l_1(x, y), \dots, l_n(x, y)$ are distinct and one of them is a positive constant. If $l_i(x, y)$ is not a constant, then $l_i(x, y) = 0$ is an equation of a line in the plane, referred to as a design line. For instance, in Fig. 2, $l_1(x, y) = x$, $l_2(x, y) = y$, $l_3(x, y) = 0.01$ so that the design lines are the coordinate axes.

Observe that function (2) vanishes only if both maxima are equal, in particular, $l_i(x, y) = l_j(x, y)$ for some $i \neq j$. The lines given by the equations $l_i(x, y) = l_j(x, y)$ for all pairs of distinct indices $i, j \in \{1, \dots, n\}$ are called equality lines. In what follows, fix such a pair $i \neq j$. For instance, in Fig. 2, the equality lines are $x = y$, $x = 0.01$, and $y = 0.01$.

Next, a point (x, y) on the equality line satisfies $f(x, y) = 0$, only if the value $l_i(x, y) = l_j(x, y)$ is maximal among $l_1(x, y), \dots, l_n(x, y)$. The intervals where

$$l_i(x, y) = l_j(x, y) \geq \max_k l_k(x, y) \quad (4)$$

are called candidate intervals. They can be straight line segments, rays, or lines. For instance, in Fig. 2, these are three rays emanating from the origin in the north-east, south, and west directions. Their union is known as the tropical line.

The candidate intervals split the plane into convex polygons, possibly empty or unbounded, given by the condition $l_i(x, y) \geq \max_k l_k(x, y)$ for some i . Each

one is referred to as the candidate polygon corresponding to the index i . In Fig. 2 on the right, the ones with $s_i < 0$ are light, and the one with $s_i > 0$ is dark.

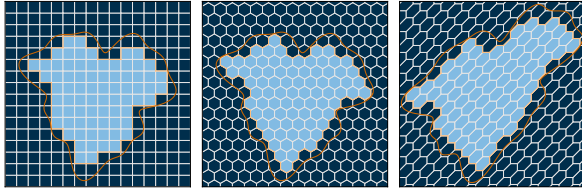


Fig. 4: Patchworks (orange) approximating a given curve (red). The construction can employ a square grid (left), a honeycomb lattice (middle), or an affine transformation of the latter (right). The squares/hexagons inside the curve are light, the other ones are dark, and the patchwork separates the colors.

Finally, to satisfy $f(x, y) = 0$, the values s_i and s_j must have opposite signs. Candidate intervals with this property are called active intervals. In Fig. 2, they are orange.

We conclude that the patchwork is the union of active intervals (if $\beta = +\infty$, some $l_i(x, y)$ is a positive constant, and the parameters are in general position; see Appendix A). The parameter β controls the sharpness of the corners. The larger β , the closer the patchwork is to this union. See Theorem 1 in Appendix A.

Expressive power. This construction allows visual control and compact representations even of complicated non-convex shapes; see Fig. 3. It also suggests the following design of a patchwork approximating a given curve; see Fig. 4.

Let the curve lie inside the box $|x|, |y| \leq 1$. Superimpose a grid of step $1/N$. Paint the squares lying inside the curve light, and the remaining ones dark. The union of the sides separating colors is called a digital curve. It can be explicitly represented as a patchwork. For notational convenience, replace the index i in (1) with a pair of indices $k, l \in [-N, N]$, so we write $a_{k,l}$ instead of a_i etc. Set

$$a_{k,l} = k, \quad b_{k,l} = l, \quad c_{k,l} = (1 - k^2 - l^2)/(2N),$$

$$s_{k,l} = \begin{cases} +1, & \text{if the candidate polygon} \\ & \text{corresponding to the pair } k, l \text{ is light,} \\ -1, & \text{otherwise.} \end{cases} \quad (5)$$

In particular, $l_{0,0}(x, y) = 1/(2N)$. The resulting candidate polygons form a square grid inside the box (this can be shown directly or using [24, Lemma 1]), and for $\beta = +\infty$, the patchwork coincides with the digital curve. For large β and N , the patchwork is close to its limiting case $\beta = +\infty$ and hence to the given curve; cf. [14, Lemma 3.8]. We conclude that any plane curve can be approximated by patchworks. See Theorem 3 in Appendix B.

There, we also discuss hexagonal lattices (see Fig. 4 on the right) and representation complexity (see Tab. 6). We can further optimize the representation; see Fig. 3.

3.2 3D

The construction in 3D is completely analogous. We represent a closed surface S as the zero level set of a field $F: \mathbb{R}^3 \rightarrow \mathbb{R}$ of a certain special form. Compared to a polygonal mesh, this gives a simple way to determine if a point x is inside S by computing the sign of $F(x)$.

Definition 2 (see Fig. 5). A patchwork field is a function $\mathbb{R}^3 \rightarrow \mathbb{R}$ of the form

$$F(x) = \frac{1}{\beta} \log \sum_{i=1}^n s_i \exp(\beta(\langle a_i, x \rangle + c_i)), \quad (6)$$

depending on the parameters $n \in \mathbb{Z}_{>0}$, $\beta \in \mathbb{R}_{>0}$, $a_i \in \mathbb{R}^3$, $c_i, s_i \in \mathbb{R}$, where $i = 1, \dots, n$. A patchwork is the surface in \mathbb{R}^3 given by $F(x) = 0$. The limiting case $\beta \rightarrow +\infty$ is

$$f(x) = \max_{i:s_i>0} \{\langle a_i, x \rangle + c_i\} - \max_{i:s_i<0} \{\langle a_i, x \rangle + c_i\}. \quad (7)$$

The surface $f(x) = 0$ is still called a patchwork.

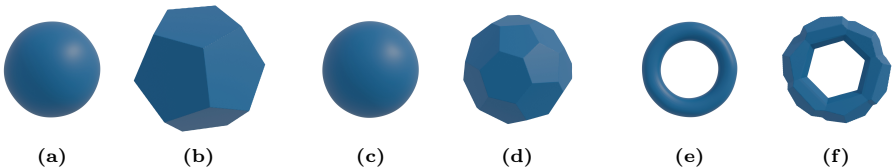


Fig. 5: Patchworks approximating a sphere (a and c) and a torus (e), and their limiting cases $\beta \rightarrow +\infty$ (b, d, f). The patchworks (a, c, e) visually coincide with the shapes, although their width is just $n = 13, 31, 30$ (left to right). For (a and b), the 12 design planes contain the faces of the dodecahedron (b), and the 13th linear function is constant. For (e and f), just 30 design planes represent an intricate nonconvex shape.

Visualization. Introduce linear functions $\mathbb{R}^3 \rightarrow \mathbb{R}$

$$l_i(x) = \langle a_i, x \rangle + c_i. \quad (8)$$

The planes $l_i(x) = 0$ (with $l_i(x) \neq \text{const}$) are called design planes. The planes $l_i(x) = l_j(x)$ for distinct $i, j \in \{1, \dots, n\}$ are called equality planes. The (possibly unbounded) convex polygons given by the conditions

$$l_i(x) = l_j(x) \geq \max_k l_k(x) \quad (9)$$

are called candidate polygons. Active polygons are the candidate polygons such that $s_i s_j < 0$. The candidate polygons decompose space into convex polyhedra

(possibly empty or unbounded) given by the condition $l_i(x) \geq \max_k l_k(x)$ for some i . These polyhedra are called **candidate polyhedra**.

For $\beta = +\infty$ and general position functions $l_i(x)$ including a positive constant, the patchwork is just the union of active polygons. For large β , the patchwork is close to the union. See Theorem 2 in Appendix A. This leads to compact surface representations; see Fig. 5. Expressive power and complexity bounds of 3D patchworks are established in Theorem 4 in Appendix B and Tab. 7 in Appendix C, respectively.

4 Optimization

Given an oriented point cloud $\{x_j, n_j\}_{j=1}^m$, where $x_j \in \mathbb{R}^3$ are points and $n_j \in \mathbb{R}^3$ are normal vectors. We aim to fit $F(x)$ such that its zero level set $\Omega_0 = \{x \in \mathbb{R}^3 | F(x) = 0\}$ describes the underlying geometry. To this end, we minimize the surface-approximation error and the normal-misalignment penalty:

$$\mathcal{L}_{\text{sur}} = \frac{1}{m} \sum_{j=1}^m |F(x_j)| \quad \text{and} \quad \mathcal{L}_{\text{normal}} = \frac{1}{m} \sum_{j=1}^m \left(1 - \frac{\nabla F(x_j) \cdot n_j}{\|\nabla F(x_j)\| \|n_j\|} \right). \quad (10)$$

To reduce off-surface parts of Ω_0 , we additionally sample m off-surface samples $\{y_k\}_{k=1}^m, y_k \in \mathbb{R}^3 \setminus \Omega_0$ per iteration for a soft occupancy regularization

$$g_{dw}(x) = 4(x - 0.5)^2 - 4|x - 0.5| + 1, \\ \mathcal{L}_{\text{reg}} = \frac{1}{m} \sum_{k=1}^m g_{dw}(\text{sigmoid}(-F(y_k)))^2, \quad (11)$$

where g_{dw} is the double-well potential [16] that attains minimum at $x = 0, 1$.

The regularization \mathcal{L}_{reg} additionally forces some candidate polyhedra to expand, leaving the other ones redundant. We hence introduce $\mathcal{L}_{\text{prune}}$ in Sec. 4.2 to progressively eliminate unnecessary ones during the fitting process.

Our total losses are

$$\mathcal{L}_{\text{total}} = \mathcal{L}_{\text{sur}} + \mathcal{L}_{\text{normal}} + \mathcal{L}_{\text{reg}} + \mathcal{L}_{\text{prune}}.$$

4.1 Explicit geometric initialization

For clarity, we consider patchwork in the following augmented form:

$$F(x) = \frac{1}{\beta^+} \log \sum_{i=1}^{n^+} \exp(\beta^+(\langle a_i^+, x \rangle + c_i^+) + \log s_i^+) \\ - \frac{1}{\beta^-} \log \sum_{i=1}^{n^-} \exp(\beta^-(\langle a_i^-, x \rangle + c_i^-) + \log s_i^-), \quad (12)$$

where $n^+ + n^- = n$, $a_i^\pm \in \mathbb{R}^3$, $c_i^\pm \in \mathbb{R}$, $s_i^\pm, \beta^\pm \in \mathbb{R}_{>0}$. Note that s_i^\pm can be losslessly incorporated into c_i^\pm , and we keep them here only for pruning purposes.

Our structure resembles 2-layer MLPs, with $[\dots a_i^\pm \dots]^T$ the weights and $[\dots c_i^\pm + \frac{\log s_i^\pm}{\beta^\pm} \dots]^T$ the biases, and the Log-Sum-Exponential (LSE) the group activation function. While the soft maximum allows gradient flow through non-maximum functions, gradient truncation, however, can still be substantial, preventing meaningful updates. Therefore, rather than relying on the standard practice of pre-specifying a hidden size and using Kaiming initialization, we propose directly initializing the parameters from the input point cloud.

From an optimization point of view, the Patchwork falls into the broad category of Difference-of-Convex (DC) problems. Specifically, its limiting form is the difference of two convex functions. Inspired by Piecewise Linear Regression (PLR) [29] in DC literature, we assign each input point x_j two linear functions (i.e., set $n^+ = n^- = m$) and force the two maxima at x_j to be attained with their corresponding coefficients $\{a_j^+, c_j^+, a_j^-, c_j^-\}$. Formally,

$$\begin{aligned} f(x) &= \max_i \{ \langle a_i^+, x \rangle + c_i^+ \} - \max_i \{ \langle a_i^-, x \rangle + c_i^- \}, \\ \arg \max_i \{ \langle a_i^+, x_j \rangle + c_i^+ \} &= \arg \max_i \{ \langle a_i^-, x_j \rangle + c_i^- \} = j. \end{aligned} \quad (13)$$

The two pointwise global-maximum constraints significantly reduce the solution space, yet the formulation remains a DC, a universal approximator.

To further reduce the solution space, we assume $f(x)$ at the initialization approximates the signed distance function. Inspired by proximal DC decomposition [31], we perform the following construction

$$h^+(x) = \frac{1}{2}\rho\|x\|^2 + \text{sdf}(x), \quad h^-(x) = \frac{1}{2}\rho\|x\|^2, \quad f(x) \approx h^+(x) - h^-(x), \quad (14)$$

where $\rho \in \mathbb{R}$ is some parameter large enough to make $h^+(x)$ convex.

Conveniently, with oriented surface samples $\{x_j, n_j\}$, we can set $f(x_j) = \text{sdf}(x_j) = 0$ and $\nabla f(x_j) = \nabla \text{sdf}(x_j) = n_j$, yielding the closed-form solution

$$\begin{aligned} a_j^+ &= \nabla h^+(x_j) = \rho x_j + n_j, & c_j^+ &= h^+(x_j) - \langle a_j^+, x_j \rangle = -\frac{1}{2}\rho\|x_j\|^2 - \langle n_j, x_j \rangle, \\ a_j^- &= \nabla h^-(x_j) = \rho x_j, & c_j^- &= h^-(x_j) - \langle a_j^-, x_j \rangle = -\frac{1}{2}\rho\|x_j\|^2. \end{aligned} \quad (15)$$

We defer the detailed derivation to Appendix D. In practice, we initialize with $\rho = 200$, $s_i^\pm = 1$, $\beta^\pm = 75$ across all our experiments. Notice the norm of a_j^\pm scales with ρ , making updating its direction stiff. So we apply weight normalization to disentangle its magnitude and direction gradient.

4.2 Progressive pruning

We propose the following loss to progressively eliminate non-contributing linear functions

$$\begin{aligned}
 w_i^\pm(x) &= \text{sg} \left(\frac{\beta^\pm(\langle a_i^\pm, x \rangle + c_i^\pm) + \log s_i^\pm}{\sum_{l=1}^{n^\pm} (\beta^\pm(\langle a_l^\pm, x \rangle + c_l^\pm) + \log s_l^\pm)} \right), \\
 \mathcal{L}_{\text{prune}}^\pm &= \frac{1}{n^\pm} \sum_{i=1}^{n^\pm} s_i^\pm + \frac{1}{m} \sum_{j=1}^m \text{ReLU} \left(1 - \sum_{i=1}^{n^\pm} s_i^\pm \cdot w_i^\pm(x_j) \right), \\
 \mathcal{L}_{\text{prune}} &= \mathcal{L}_{\text{prune}}^+ + \mathcal{L}_{\text{prune}}^-,
 \end{aligned} \tag{16}$$

where sg is the stop gradient operator, and w_i^\pm can be viewed as a typical soft maximum. The first term encourages all s_i^\pm to be diminished, while the second term maintains the magnitude of s_i^\pm that contributes to candidate polygons.

For every fixed iterations, we detect linear functions with $s_i^\pm < 10^{-2}$, and disable them softly by setting $s_i^\pm = 10^{-5}$.

4.3 Fully-fused kernel acceleration

For n linear functions and m samples, a naive computation of LSE in (12) or the soft maximum in (16) would both materialize the $\mathbb{R}^{n \times m}$ dot product matrix, resulting in $\mathcal{O}(nm)$ memory complexity. Inspired by the FlashAttention [6] style kernel implementation in `efunc` [40], we fuse the two operations into a single kernel, while reducing the memory complexity to $\mathcal{O}(m)$. For $n = m = 16384$, our fused implementation reduces the intermediate memory footprint of the two operators from 2.15 GB to 65.8 KB in the forward pass, and from 2.14 GB to 394 KB in the backward pass.

4.4 Implementation details

We normalize shapes in datasets to $[-1, 1]$ and uniformly sample m surface points with face normals, with m depending on the experiment setup. For each iteration, we additionally sample m off-surface points for regularization. For each shape, we run 10k iterations with a batch size of 16384 using the Adam optimizer with a learning rate of 10^{-3} on a single RTX3090 GPU (24 GB VRAM). We perform pruning every 2K iterations. We implement training code using JAX [3] and fused kernel using Triton [34]. The fitting takes around 1.5 minutes for $m = 1024$ and 5 minutes for $m = 16384$. Our full implementation is available at <https://github.com/Ankbzpx/patchwork-experiment>.

5 Results

To demonstrate our compactness and expressiveness, we present a comparison of competing representations of the matching parameter size with our *overparameterized* initialization. In addition, we ablate our design choices, present a discussion, and leave future work to Appendix G.

Table 1: Quantitative results on the roof modeling dataset. The bold text indicates the best score. To approximate the SPSR parameter count, we voxelize input clouds over sparse octrees of the same depth, then average the number of nodes. Ours is the average parameter size after the progressive pruning. CH=Chamfer; HD=Hausdorff; FS=F-score.

Method	CH ↓	HD ↓	FS ↑	# Params
MC	6.79	8.68	49.93	8000
RFTA	3.62	5.88	36.83	8000
SPSR	5.55	7.20	19.66	8806
VoroMesh	17.27	16.81	7.95	8000
PoNQ	8.01	13.44	53.61	8800
SIREN	22.57	77.28	51.52	8641
Ours init	18.11	62.52	60.16	8192
Ours	1.42	1.45	76.88	1301

5.1 Dataset

Roof modeling As explained earlier, the main advantage of our method is its compactness—using only a few planes, we can assemble complex shapes, with the number of planes corresponding exactly to the candidate polyhedra. Therefore, we compare our representation on the Roof-Image dataset [25], consisting of 3K unique building roof meshes, each with a structure composed of simple yet diverse and topologically complex polygons. We randomly select 200 cases, normalize them to the range $[-1, 1]$, and sample $m = 1024$ points without further processing.

ABC and Thingi10k To further evaluate our expressiveness in handling more general shapes, we additionally choose two widely used datasets, ABC [15] and Thingi10k [42], the former is a large collection of CAD models, while the latter consists of 10K more general shapes. We pick 100 models from each, following the common test split [8, 10], normalize them to $[-1, 1]$ and set sample size to $m = 16384$.

5.2 Comparisons

We compare 3D representation with other common, topology-agnostic ones in deep learning, namely regular grids, point clouds, and MLPs. For fairness, we configure those to match the parameter sizes of our *overparameterized* initialization. Consequently, we ignore s_i^\pm , which is used solely for pruning, and count our parameter size as $8m$, where m is the surface sample size.

Regular grid Given an SDF grid, the de facto way of extracting the underlying surface is Marching Cube (MC) [17], yet it overlooks the SDF’s spherical property [27], hence underutilizes the stored information. Reach for the Arc (RFTA) [26] explicitly exploits this property and achieves the state-of-the-art performance at

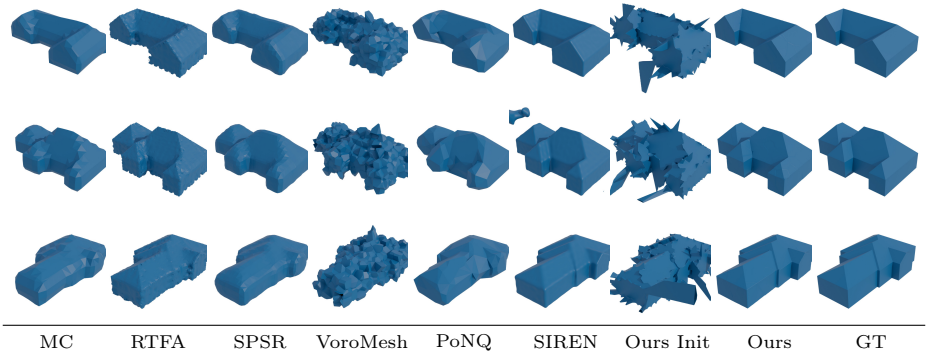


Fig. 6: Qualitative results on the roof modeling dataset. Our method has clear advantages both in visual quality and compactness.

recovering high-quality surfaces from discrete grids. We compare both MC and RTFA on a fixed-dimensional grid of 20^3 for the Roof modeling dataset and 50^3 for ABC and Thingi10k, with SDFs calculated from ground-truth data to ensure accuracy and fairness.

Point cloud We compare the axiomatic method of surface reconstruction from oriented point cloud, the Screened Poisson Surface Reconstruction (SPSR) [13]. We estimate its memory complexity and set depth to 6 for the Roof modeling dataset and depth to 8 for ABC and Thingi10k, while using the same input point clouds as ours. VoronMesh [20] fits double covering point clouds as Voronoi generators and extracts crossing boundaries as a reconstructed mesh. Since they initialize generators using voxel centers, we use 20^3 for the Roof modeling dataset and 50^3 for ABC and Thingi10k. PoNQ [21] associates each oriented sample with a $\mathbb{R}^{4 \times 4}$ quadric matrix to guide triangulation. To account for extra parameters per sample, we set $m = 400$ for the Roof modeling dataset and $m = 6000$ for ABC and Thingi10k.

MLP Neural implicit representation uses coordinate MLPs to encode SDFs as continuous functions, hence requiring high expressiveness to model discrete jumps such as sharp edges. We choose SIREN [30] as a baseline as it facilitates learning high-frequency signals. We use 2 hidden layers of 64 units for the Roof modeling dataset (i.e., 2 weight matrices in $\mathbb{R}^{64 \times 64}$), and with 2 hidden layers of 256 units for ABC and Thingi10k (i.e., 2 weight matrices in $\mathbb{R}^{256 \times 256}$).

Metrics For quantitative evaluation, we sample 1M points on both ground truth and extracted surface and report Chamfer Distance ($\times 10^{-3}$), Hausdorff distance ($\times 10^{-2}$), and F-score with a cutoff 0.1% maximum dimension of the bounding box. For our method and MLP, we use MC of resolution 512^3 to extract the underlying surfaces.

Table 2: Quantitative results on ABC / Thingi10K. The bold text indicates the best score; the underlined text indicates the second-best. To approximate the SPSR parameter count, we voxelize input clouds over sparse octrees of the same depth, then average the number of nodes. Ours is the average parameter size after the progressive pruning. CH=Chamfer; HD=Hausdorff; FS=F-score.

Method	CH ↓	HD ↓	FS ↑	# Params
MC	4.61 / 3.56	6.00 / 6.78	48.10 / 43.82	125000
RFTA	3.82 / 12.92	5.60 / 7.15	53.09 / 53.51	125000
SPSR	<u>2.49</u> / 2.02	3.77 / 4.32	58.01 / 63.21	150975
VoroMesh	5.95 / 3.62	6.94 / 6.65	36.99 / 42.17	125000
PoNQ	3.30 / 2.87	5.82 / 6.20	<u>58.59</u> / 51.79	132000
SIREN	2.79 / 3.18	25.32 / 26.24	57.25 / 61.28	132865
Ours init	5.53 / 11.44	21.53 / 40.69	54.10 / 56.68	131072
Ours	2.48 / <u>2.39</u>	<u>4.93</u> / <u>5.88</u>	60.83 / <u>61.59</u>	6262

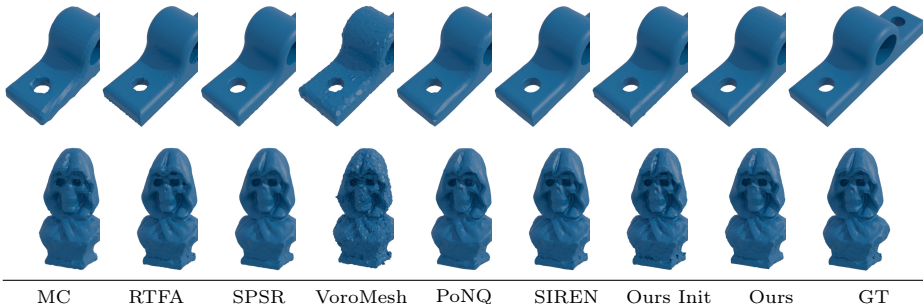


Fig. 7: Qualitative results on the ABC and Thingi10k datasets. Our method can compactly represent CAD and general shapes.

5.3 Discussion

For the roof modeling dataset, as illustrated in Fig. 6 and Tab. 1, our method surpasses all others by a large margin while requiring only a fraction of as many parameters. Interestingly, our initialization, although exhibiting some surplus parts (as measured by Chamfer and Hausdorff distances), more closely resembles the target shape than all other methods (as measured by F-score).

For ABC and Thingi10 (Fig. 7, Tab. 2), our method achieves the best for ABC in terms of Chamfer distance and F-score, and the second best for all other metrics, while requiring only half the parameters. For Thingi10k, our performance is relatively lower because we have two failure cases (with F-scores close to 0), which we discuss in detail in Appendix F. See more results in Figs. 9–13.

Table 3: Ablation study of our explicit geometric initialization on roof modeling / ABC / Thingi10k datasets.

	Chamfer ↓	Hausdorff ↓	F-score ↑
w.o.	14.33 / 61.73 / 59.00	18.20 / 40.24 / 41.46	29.87 / 8.16 / 3.98
w.	1.42 / 2.48 / 2.39	1.45 / 4.93 / 5.88	76.88 / 60.83 / 61.59

5.4 Ablation studies

Explicit geometric construction We ablate the effectiveness of geometric w.r.t. Kaiming initialization (Tab. 3). Without geometric initialization, the soft maximum renders most parameters dead, preventing fitting of any meaningful shapes.

Table 4: Ablation study of \mathcal{L}_{sur} , $\mathcal{L}_{\text{normal}}$, and \mathcal{L}_{reg} on the roof modeling dataset.

\mathcal{L}_{sur}	$\mathcal{L}_{\text{normal}}$	\mathcal{L}_{reg}	Chamfer ↓	Hausdorff ↓	F-score ↑
✓	✗	✗	132.68	115.16	3.36
✓	✓	✗	57.49	83.27	39.92
✓	✗	✓	1.56	2.06	76.79
✗	✗	✓	496.99	114.51	0.05
✗	✓	✓	503.22	132.20	0.09
✓	✓	✓	1.42	1.45	76.88

Losses We further ablate our three losses, \mathcal{L}_{sur} , $\mathcal{L}_{\text{normal}}$, and \mathcal{L}_{reg} . As shown in Tab. 4, both \mathcal{L}_{sur} and \mathcal{L}_{reg} are essential for bounding the geometry, while $\mathcal{L}_{\text{normal}}$ help improve accuracy.

Progressive Pruning Lastly, we ablate the effect of progressive pruning in Tab. 5. Pruning diminishes the weights of covered parts, forcing the optimizer to attend to contributing linear functions and thereby improving performance. Moreover, as shown in the Sec. 5.2, pruning substantially reduces our parameter count.

Table 5: Ablation study of progressive pruning on the roof modeling dataset.

N	Chamfer ↓	Hausdorff ↓	F-score ↑
w.o.	1.69	1.90	76.71
w.	1.42	1.45	76.88

6 Conclusions

We propose a highly compact shape representation for 3D shapes. It is designed to be compatible with neural networks and is particularly effective for representing coarse, man-made shapes and CAD models. We bring in *Viro's patchworking* construction from pure mathematics and refine it by introducing arbitrary real weights, thus achieving a fixed number of real parameters in the representation. Our results show significant improvements compared to current SOTA 3D shape representations.

Acknowledgements

The research reported in this publication was supported by funding from King Abdullah University of Science and Technology (KAUST) – Center of Excellence for Generative AI, under award number 5940 and a gift from Google.

A Dependence on the parameters

In this supplementary material, we discuss the dependence of the patchwork on the parameters and clarify the technical assumptions required for Section 3 above. The derivations there are valid in general position, that is, unless the parameters satisfy certain specific relations. We show that a general position patchwork $f(x, y) = 0$ is a limiting case of $F(x, y) = 0$ as $\beta \rightarrow +\infty$; see Fig. 2.

More precisely, under notation (2)–(3), we say that $a_i, b_i, c_i, s_i \in \mathbb{R}$ are general position parameters including a positive constant, if the following conditions hold:

- for some index i , we have $l_i(x, y) = \text{const} > 0$, $s_i \neq 0$;
- for distinct indices i , the functions $l_i(x, y)$ are distinct;
- for any triple of distinct indices i, j, k , the equation $l_i(x, y) = l_j(x, y) = l_k(x, y)$ has finitely many solutions;
- for any four distinct indices i_1, \dots, i_4 , the equation $l_{i_1}(x, y) = \dots = l_{i_4}(x, y)$ has no solutions.

By the argument in Section 3, for general position parameters including a positive constant, the patchwork $f(x, y) = 0$ is the union of active segments. Here, none of the conditions can be dropped. For instance, for $l_1(x, y) = x$, $l_2(x, y) = y$, $l_3(x, y) = 1$, $l_4(x, y) = (x + y + 1)/3$, $s_1 = s_2 = s_3 = -s_4 = 1$ (violating the last condition), the set $f(x, y) = 0$ consists of a single point $(1, 1)$, whereas there are no active segments. The following theorem holds.

Theorem 1 (Tropical limit). *Under notation (1)–(3), for any general position parameters including a positive constant, the Hausdorff distance between the sets given by $F(x, y) = 0$ and $f(x, y) = 0$ tends to zero as $\beta \rightarrow +\infty$.*

Proof. Consider the ε -neighborhood U of the patchwork $f(x, y) = 0$ for some $\varepsilon > 0$ and the candidate polygon P_i corresponding to an index i . It suffices to show that the sign of $e^{\beta F(x, y)} - 1$ in $P_i \setminus U$ is the same as the sign of s_i for sufficiently large β . Clearly, then the Hausdorff distance between the sets given by $F(x, y) = 0$ and $f(x, y) = 0$ is $O(\varepsilon)$ and tends to zero as $\beta \rightarrow +\infty$.

We start with showing that $f(x, y)$ is bounded from 0 in $\mathbb{R}^2 \setminus U$. Indeed, take a box B containing all pairwise intersections of equality lines. The complement to $B \cup U$ can be covered by rays starting at the boundary of B and not crossing the equality lines. On each ray, $f(x, y)$ is linear and non-vanishing. Hence, $|f(x, y)|$ attains a minimum at the starting point. By compactness, there is $\delta = \delta(\varepsilon) > 0$ such that $|f(x, y)| > \delta$ in $B \setminus U$, hence in $\mathbb{R}^2 \setminus U$.

Next, take $(x, y) \in P_i \setminus U$. By definition, the sign of $f(x, y)$ is the same as the sign of s_i . Assume that $s_i > 0$ (the other case is analogous). Then $f(x, y) > \delta$. Pick any

$$j \in \arg \max_{k: s_k < 0} \{l_k(x, y)\}.$$

Then $l_i(x, y) > \delta + l_j(x, y)$. Since some $l_k(x, y) = c > 0$ is a positive constant, it follows that $l_i(x, y) \geq c$. Then

$$\begin{aligned} e^{\beta F(x, y)} &= \sum_{k: s_k > 0} s_k e^{\beta l_k(x, y)} - \sum_{k: s_k < 0} |s_k| e^{\beta l_k(x, y)} \\ &\geq \begin{cases} (s_i e^{\beta \delta} - \sum_k |s_k|) e^{\beta l_j(x, y)}, & \text{if } l_j(x, y) \geq 0, \\ (s_i e^{\beta c} - \sum_k |s_k|), & \text{if } l_j(x, y) < 0, \end{cases} \end{aligned} \quad (17)$$

We conclude that $e^{\beta F(x, y)} > 1$, once

$$\beta > \frac{1}{\min\{\delta, c\}} \log \frac{\sum_k |s_k| + 1}{\min_{k: s_k \neq 0} \{|s_k|\}}. \quad (18)$$

Analogously, $e^{\beta F(x, y)} < 1$ in $P_i \setminus U$ for $s_i < 0$. QED

Let us give a few remarks on the dependence on the parameters other than β . The change of a_i, b_i, c_i, s_i affects only the boundary of the candidate polygon corresponding to index i , and hence is a local change of the patchwork $f(x, y) = 0$. The changes to the patchwork $F(x, y) = 0$ exponentially decrease with distance from the polygon. When s_i passes through 0, the polygon is abruptly added to or removed from the ‘‘interior’’ of the patchwork $f(x, y) = 0$. For the patchwork $F(x, y) = 0$, this jump is smeared out.

In 3D, we say that $a_i \in \mathbb{R}^3$ and $c_i, s_i \in \mathbb{R}$ are general position parameters including a positive constant, if

- for some index i , we have $l_i(x) = \text{const} > 0$ and $s_i \neq 0$;
- for any $k \geq 2$ distinct indices i_1, \dots, i_k , we have

$$\dim\{x \in \mathbb{R}^3 : l_{i_1}(x) = \dots = l_{i_k}(x)\} \leq 4 - k. \quad (19)$$

For such parameters, the patchwork $f(x) = 0$ is the union of active polygons. The following theorem is proved analogously to Theorem 1.

Theorem 2 (Tropical limit). *Under notation (6)–(8), for any general position parameters including a positive constant, the Hausdorff distance between the sets given by $F(x) = 0$ and $f(x) = 0$ tends to zero as $\beta \rightarrow +\infty$.*

B Expressive power

In this supplementary material, we demonstrate the expressive power of patchworks: first, in 2D, then, in 3D.

Theorem 3 (Expressive power). *For any Jordan curve and any $\varepsilon > 0$, there exists a patchwork within the Hausdorff distance ε from the curve. For a smooth curve, there is a patchwork of width $O(1/\varepsilon^2)$ with this property.*

Here, roughly speaking, a Jordan curve is a closed, continuous curve without self-intersections. More precisely, a Jordan curve is the image of an injective continuous map of a circle into the plane. A Jordan curve need not be smooth, so that the theorem applies to fractal curves as well. The generalization to curves having finitely many disjoint components is straightforward. Thus, we obtain a method to approximate essentially any plane curve by a patchwork.

Note that any continuous piecewise linear function can be represented in form (2); see [29]. Hence, any polyline without self-intersections or disjoint union of such polylines, can be represented as a patchwork. The advantage of our method is a simple, explicit expression for the parameters.

Proof. We prefer to use a hexagonal lattice for approximation. Replace the index i in (1) with a pair of indices $k, l \in [-N, N]$, so we write $a_{k,l}$ instead of a_i etc. Consider a patchwork with parameters

$$a_{k,l} = k, \quad b_{k,l} = l, \quad c_{k,l} = -(k^2 + l^2 + kl - 1)/N, \quad s_{k,l} \in \{+1, -1\}. \quad (20)$$

The resulting candidate polygons are hexagons with the sides parallel to the lines $x = 0$, $y = 0$, and $x = y$. They form an affine-transformed honeycomb lattice; see Fig. 4 on the right. For $\beta = +\infty$, the resulting patchwork (that is, the union of polylines separating candidate polygons corresponding to the indices k, l with $s_{k,l}$ of opposite signs) is called a hex-curve (of step $1/N$).

It suffices to prove Theorem 3 for a smooth curve, because any Jordan curve can be approximated by smooth ones in Hausdorff distance. By [14, Lemma 3.8], for any smooth Jordan curve, there is a constant C (depending on the curve) such that for any sufficiently small mesh step $\delta > 0$ there is a hex-curve of step δ within Hausdorff distance $C\delta$ from the smooth curve. For $\delta < \varepsilon/C$, the hex-curve is within Hausdorff distance ε . Assume WLOG that the smooth curve lies in the box $|x|, |y| < 1$. Then the hex-curve is the patchwork with parameters (20) and has width at most $(2/\delta)^2 = O(1/\varepsilon^2)$, as required. QED

Note that for a non-smooth curve, the Hausdorff distance to the hex-curve can decrease with $\delta \rightarrow 0$ slower than any linear function in δ [14, Remark after Lemma 3.8].

As a byproduct, our representation allows direct sampling of certain complicated random fractals. Namely, if one paints the hexagons of a honeycomb lattice in two colors randomly with equal probabilities independently of each other, then the hex-curve approximates a random fractal known as CLE_6 [22]. Patchwork parameters (20) can be easily modified to represent the hex-curve (before the affine transformation of the honeycomb lattice) and thus to sample the random CLE_6 fractal. Other random fractals arising from sampling random patchworks can also be of interest and are the subject of future work.

Another side remark is that the relation between the patchwork parameters and the tessellation by candidate polygons is most visual in the context of isotropic geometry and metric duality; see [24, Section 2] for an introduction.

Now we proceed to the 3D case. Let us approximate a given surface $S \subset [-1, 1]^3$ by a patchwork. Take an integer N and replace the index i in (6) with

a triple of indices $k, l, m \in [-N, N]$, so we write $a_{k,l,m}$ instead of a_i etc. Set

$$\begin{aligned} a_{k,l,m} &= (k, l, m), & c_{k,l,m} &= \frac{1 - k^2 - l^2 - m^2}{2N}, \\ s_{k,l,m} &= \begin{cases} -1, & \text{if } (k, l, m)/N \text{ is inside } S, \\ +1, & \text{otherwise.} \end{cases} \end{aligned} \quad (21)$$

The resulting candidate polygons are squares forming a cubic grid. For $\beta = +\infty$, the patchwork is the union of the squares separating cube midpoints inside and outside S . This union is called a digital surface. For large β and N , the patchwork is close to the digital surface and hence to S . We arrive at the following theorem.

Theorem 4 (Expressive power). *Any compact embedded surface without boundary in \mathbb{R}^3 can be approximated by patchworks, that is, for each $\varepsilon > 0$, there exists a patchwork within the Hausdorff distance ε from the surface.*

Here, by a compact embedded surface without boundary, we mean the image of an injective continuous map of a compact two-dimensional manifold into \mathbb{R}^3 . The manifold need not be connected, and the map need not be smooth.

Proof. It suffices to show that the Hausdorff distance between the initial surface S and the digital surface D tends to zero as $\delta \rightarrow 0$, because any digital surface is a patchwork with parameters (21). Consider the set S_δ of points inside S at a distance $\geq 2\delta$ from it. All those points lie in the cubes inside S ; otherwise, there would be a cube of diameter $\sqrt{3}\delta$ intersecting both S and S_δ . All the points outside of S lie in the cubes, not inside S . Thus, D lies between S and S_δ , and the Hausdorff distance between S and D is not greater than the one between S and S_δ . The latter distance tends to zero as $\delta \rightarrow 0$: indeed, applying Dini's theorem to the functions $f_\delta: S \rightarrow \mathbb{R}$, $x \mapsto \text{dist}(x, S_\delta)$, we conclude that $\max_{x \in S} f_\delta(x) \rightarrow 0$ as $\delta \rightarrow 0$. QED

C Representation complexity

Now we address the question of the representation complexity of patchworks, that is, what complexity of patchworks is required to represent the shape of given complexity. Remarkably, for some complexity measures, we can achieve lower bounds and thus contribute to the famous problem of lower bounds in computational complexity theory.

In this work, we focus on a single toy example of a complexity measure to provide a proof of concept for patchwork complexity lower bounds. Namely, we study rough bounds on the numerical precision (the number of digits in the decimal representation) of the patchwork coefficients a_i and b_i (a_i in the 3D case) required to represent a given shape. So far, we have not attempted to bound the width n , which is a more natural but more complicated complexity measure for the analysis, to be addressed in future work.

Without loss of generality, we assume that all the coefficients a_i and b_i are integers, because we can always scale them by a common factor and absorb it into β , without changing the patchwork. We also assume that they are non-negative, because we can always add a common constant to them. Then, introduce the patchwork precision complexity

$$M := \max_i \{a_i, b_i\}. \quad (22)$$

The value $\log_{10} M$ roughly measures the numerical precision of the coefficients before scaling and adding a constant.

Analogously, in 3D, denote $a_i = (a_{i,1}, a_{i,2}, a_{i,3})$, assume $a_{i,j} \in \mathbb{Z}_{\geq 0}$ for all i, j , and set

$$M := \max_{i,j} \{a_{i,j}\}. \quad (23)$$

Table 6: A few lower bounds on the precision complexity M of a patchwork representing a given bounded curve. The x -projection degree D is the maximal number of intersections of the curve with an y -parallel line. See Section C for details.

Curve complexity measure	Notation	Bound	Underlying theorem
x -projection degree	D	$M \geq D$	Bézout's theorem
number of components	C	$M \geq \sqrt{2C}$	Harnack's curve theorem

Table 7: A few lower bounds on the precision complexity M of a patchwork representing a given closed surface. The xy -projection degree D is the maximal number of intersections of the surface with a z -parallel line. The number of handles G is the total genus of all the surface components. See Section C for details.

Surface complexity measure	Bound	Underlying theorem
xy -projection degree	D $M \geq D$	Bézout's theorem
number of components	C $M \geq \sqrt[3]{2C}$	Generalized Harnack Inequality
number of handles	G $M \geq \sqrt[3]{2(C+G)}$	[12] and Proposition 1

In Tables 6–7, we collect a few lower bounds on M for a patchwork with finite β and all $a_i, b_i \in \mathbb{Z}_{\geq 0}$ (or $a_{i,j} \in \mathbb{Z}_{\geq 0}$) representing a given shape. They come from the observation that the exponential map $(x, y) \mapsto (e^{\beta x}, e^{\beta y})$ takes the patchwork to an algebraic set of degree M , and the known theorems on the complexity of the latter.

Conversely, if for some $\beta > 0$, the exponential map takes a given set to an algebraic hypersurface of degree M , then the set is a patchwork of precision complexity M . This is a toy example of a patchwork complexity upper bound.

Specifically, in Tables 6–7, we use Bézout's and Harnack's theorem, and the following folklore one.

Proposition 1 (Algebraic surface complexity bound). *Consider a bounded algebraic surface of degree M in \mathbb{R}^3 with C components and the sum G of the genera of all components. Assume that the extension of the algebraic surface to complex projective space is smooth. Then*

$$M(M^2 - 4M + 6) \geq 2(C + G). \quad (24)$$

Proposition 1 follows from known results surveyed in [12], but the proof requires familiarity with basic topology and algebraic geometry.

Proof. Since the algebraic surface is bounded and non-singular, it is a disjoint union of finitely many closed compact orientable surfaces, and its projective closure in real projective space has the same topological type. Then the projective closure has the sum $C + 2G + C$ of the Betti numbers over $\mathbb{Z}/2\mathbb{Z}$. By the Generalized Harnack Inequality [12, Theorem 1.1], this sum is not greater than the analogous sum for the extension (Zariski closure) to the complex projective space. By the known computation (see e.g., [38] or [12, p. 93]), the latter sum equals $M(M^2 - 4M + 6)$, and the desired inequality follows. QED

D Geometric initialization

In this supplementary material, we derive geometric initialization (15) from assumptions (13). We start with introducing the functions

$$f^\pm(x) = \max_i \{\langle a_i^\pm, x \rangle + c_i^\pm\}. \quad (25)$$

By our assumptions (13), the maximum for $x = x_j$ is attained at $i = j$. Then it is natural to assume that for x sufficiently close to x_j , we still have

$$f^\pm(x) = \langle a_j^\pm, x \rangle + c_j^\pm \quad (26)$$

and hence

$$\nabla f^\pm(x) = a_j^\pm. \quad (27)$$

Substituting $x = x_j$, we get

$$f^\pm(x_j) = \langle a_j^\pm, x_j \rangle + c_j^\pm \quad \text{and} \quad \nabla f^\pm(x_j) = a_j^\pm. \quad (28)$$

Recall definition (14) of convex functions

$$h^+(x) = \frac{1}{2}\rho\|x\|^2 + \text{sdf}(x) \quad \text{and} \quad h^-(x) = \frac{1}{2}\rho\|x\|^2. \quad (29)$$

To satisfy

$$f(x_j) = \text{sdf}(x_j) = 0 \quad \text{and} \quad \nabla f(x_j) = \nabla \text{sdf}(x_j) = n_j, \quad (30)$$

it is natural to require the conditions

$$f^\pm(x_j) = h^\pm(x_j) \quad \text{and} \quad \nabla f^\pm(x_j) = \nabla h^\pm(x_j). \quad (31)$$

Comparing with equation (28), we get the desired closed-form solution (15):

$$\begin{aligned} a_j^+ &= \nabla h^+(x_j) = \rho x_j + n_j, & c_j^+ &= h^+(x_j) - \langle a_j^+, x_j \rangle = -\frac{1}{2}\rho \|x_j\|^2 - \langle n_j, x_j \rangle, \\ a_j^- &= \nabla h^-(x_j) = \rho x_j, & c_j^- &= h^-(x_j) - \langle a_j^-, x_j \rangle = -\frac{1}{2}\rho \|x_j\|^2. \end{aligned} \quad (32)$$

The resulting solution automatically satisfies assumptions (13): The plot of linear function (26) is the tangent plane to the plot of the convex function $h^\pm(x)$ at the point $x = x_j$. Thus, the maximum in (25) for $x = x_j$ is attained at $i = j$.

E Explicit extraction

Our method supports explicit extraction of the patchwork (for $\beta = +\infty$), that is, the union of active segments (in 2D) or active polygons (in 3D); see Fig. 8. For each interior candidate polygon/polyderon (i.e., corresponding to an index i with $s_i < 0$), compute the equality lines/planes $\langle a_i, x \rangle + c_i = \langle a_j, x \rangle + c_j$ for all $j = 1, \dots, n$ (i.e., the halfspaces that bound the current candidate polygon). Then find its Chebyshev center x by maximizing y over all pairs (x, y) satisfying the constraint

$$\langle a_j - a_i, x \rangle + y \|a_j - a_i\|_2 + c_j - c_i \leq 0, \quad \forall j \in [n]. \quad (33)$$

If the resulting $y > 0$, then compute the intersections of those halfspaces. Then we compute the convex hull and determine connectivity. After performing the same for all interior candidate polygons/polydera, we identify all active segments/polygons for the final patchwork extraction.

We use Marching Cubes for the main results because explicit extraction does not preserve the smoothness induced by the soft maximum.

F Failure cases

As illustrated in Fig. 12, we have two failure cases resulting in close to zero F-score for the Thing10K dataset. The first case (top row) has two layers of surfaces of the same normal orientations. Our initialization creates many cracks that cannot be resolved. The second case (bottom row) has many intricate isolated parts, for which our sampling and losses are insufficient to bound our initialization.

G Future work

We propose the following future work addressing the theory and applications of the proposed representation.

Theory: Patchworks represent either smooth (for finite β) or piecewise-linear shapes (for $\beta = +\infty$). It is interesting to modify the construction to allow sharp corners and edges for non-piecewise-linear curves and surfaces. It is interesting to

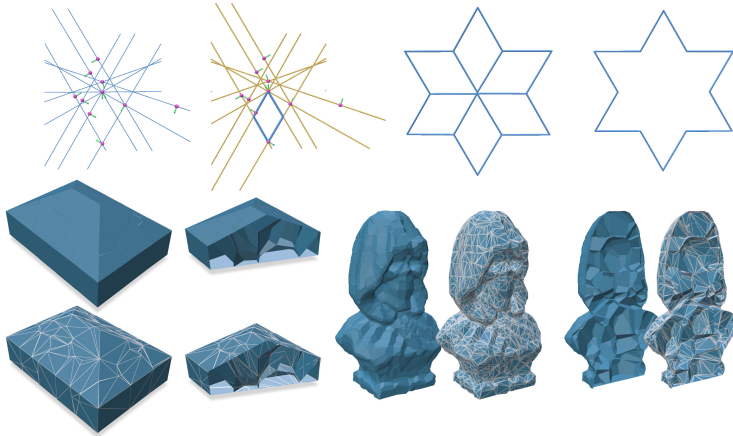


Fig. 8: Explicit extraction. The top row illustrates the patchwork extraction procedure, from left to right: 1) equality lines; 2) halfspace intersections with connectivity; 3) resulting interior candidate polygons; 4) resulting active segments. The bottom row shows extractions, interior candidate polyhedra, and tessellations for 3D cases. We use Qhull [2] for convex hull computation and Polycopo [28] for visualization.

get bounds on the precision complexity and width of the patchwork representation of a shape; for instance, to determine if the maximal number of intersections of the shape with a line is a lower bound on both. Furthermore, we conjecture that the upper bound $O(1/\varepsilon^2)$ on the width described in Theorem B.1 in the supplementary material can be improved to $O(1/\varepsilon)$.

Initialization and Expansion: Our current implementation relies on a faithful initialization, with \mathcal{L}_{sur} , $\mathcal{L}_{\text{normal}}$, and \mathcal{L}_{reg} bounding and refining the initialization, while the side effect of \mathcal{L}_{reg} gradually expands polyhedra acrossing zero level set to cover non-contributing ones. When our initialization failed, or when the samples are insufficient to bound the geometric details, our method can produce inaccurate reconstructions, as illustrated by our two failure cases. There are also cases where details of our initialization get blurred out in the expansion procedure, such as the bottom row of Fig. 11. We anticipate that developing more robust initialization and expansion schemes will improve our robustness, enabling our method to fully realize its theoretical expressiveness.

Applications: The most important applications are in the area of low complexity shape modeling. Specifically, we believe that the representation is very promising for generative modeling of man-made objects and for the 3D reconstruction of shapes from point clouds and images. This would require assembling a larger dataset of 3D shapes in the newly proposed representation and training a diffusion model.

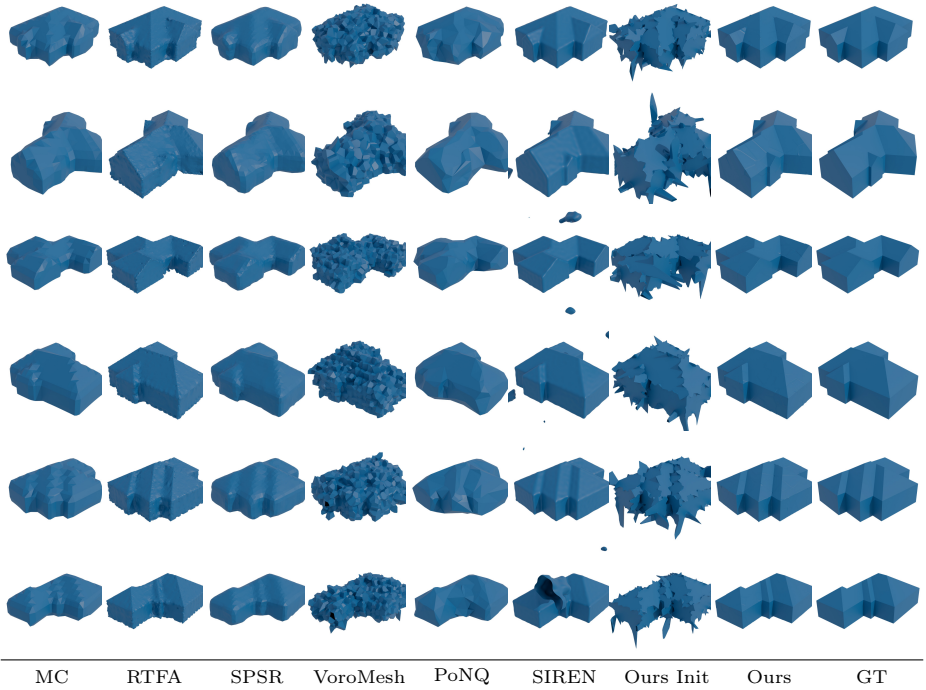


Fig. 9: More qualitative results on the roof modeling dataset.

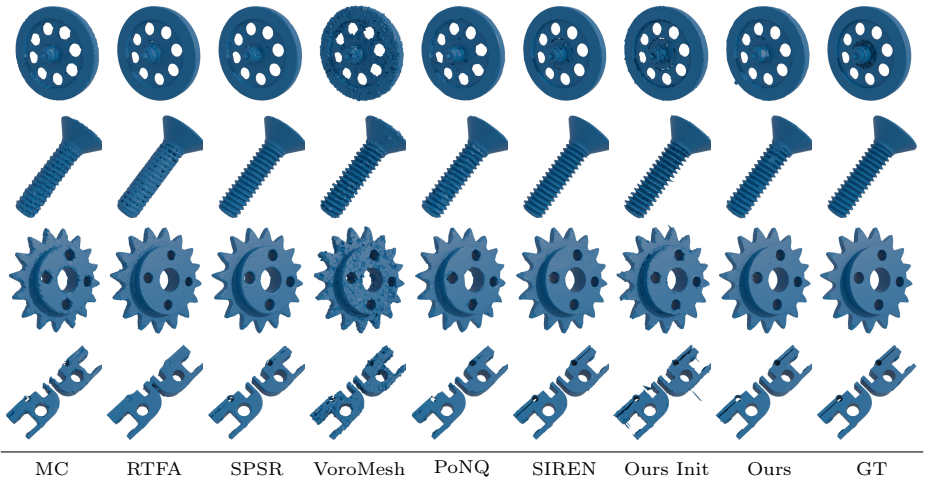


Fig. 10: More qualitative results on the ABC dataset.

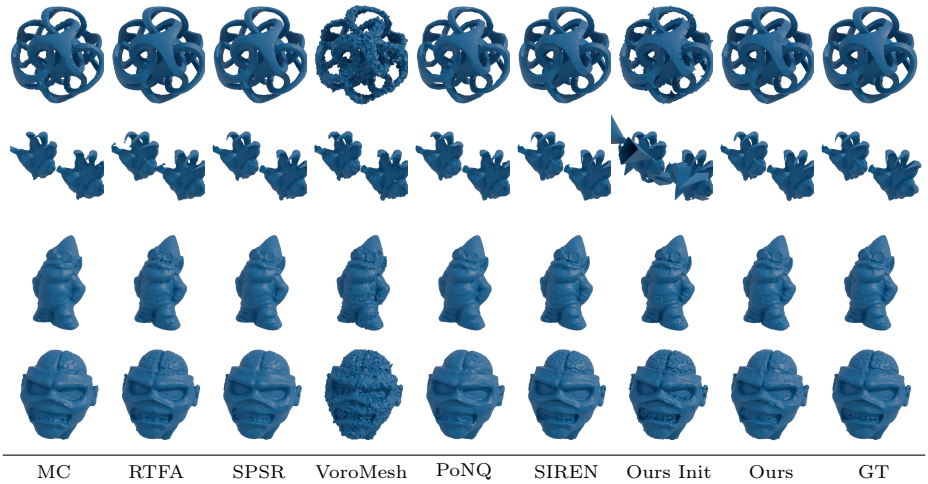


Fig. 11: More qualitative results on the Thingi10K dataset.

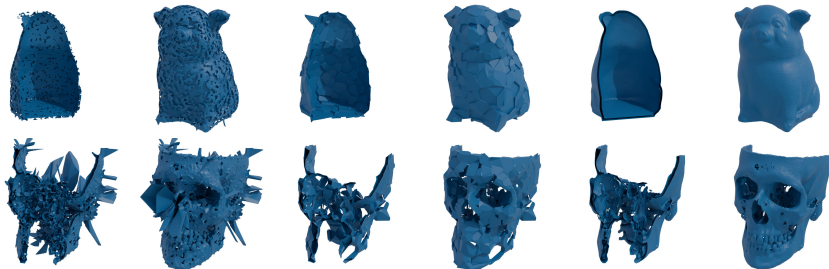


Fig. 12: Two failure cases of our method. Per row, from left to right, the pairs correspond to Ours Init, Ours, and GT.

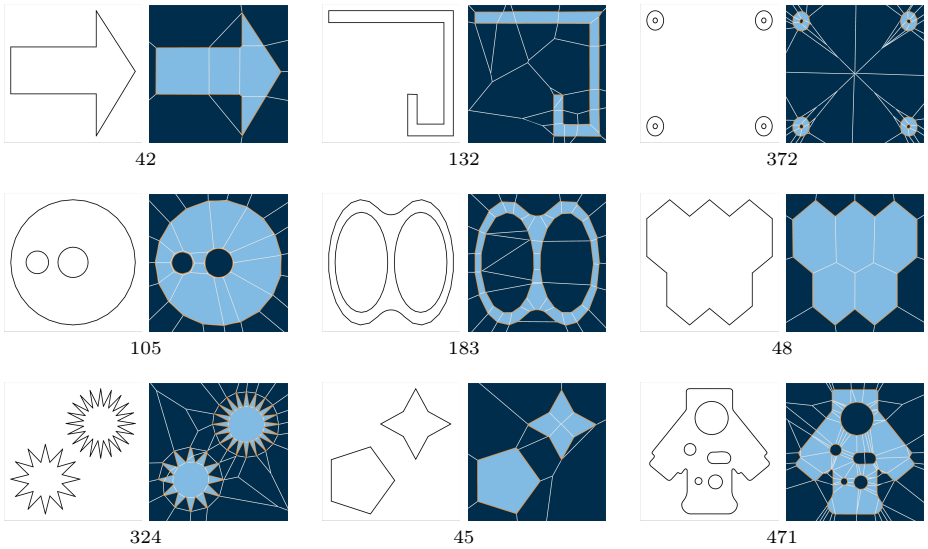


Fig. 13: Some 2D examples. Numbers indicate the number of parameters (i.e., $3 \times$ the number of design lines) needed to represent them as a patchwork.

References

1. Alfarra, M., Bibi, A., Hammoud, H., Gaafar, M., Ghanem, B.: On the decision boundaries of neural networks: A tropical geometry perspective. *IEEE Transactions on Pattern Analysis and Machine Intelligence* **45**(4), 5027–5037 (2022) 4
2. Barber, C.B., Dobkin, D.P., Huhdanpaa, H.: The quickhull algorithm for convex hulls **22**(4), 469–483 (Dec 1996). <https://doi.org/10.1145/235815.235821>, <https://doi.org/10.1145/235815.235821> 23
3. Bradbury, J., Frostig, R., Hawkins, P., Johnson, M.J., Leary, C., Maclaurin, D., Necula, G., Paszke, A., VanderPlas, J., Wanderman-Milne, S., Zhang, Q.: JAX: composable transformations of Python+NumPy programs (2018), <http://github.com/google/jax> 10
4. Brandenburg, M.C., Loho, G., Montufar, G.: The real tropical geometry of neural networks for binary classification. *Transactions on Machine Learning Research* (2024) 3, 4
5. Chen, Z., Tagliasacchi, A., Zhang, H.: Bsp-net: Generating compact meshes via binary space partitioning. In: *Proceedings of the IEEE/CVF conference on computer vision and pattern recognition*. pp. 45–54 (2020) 4
6. Dao, T., Fu, D., Ermon, S., Rudra, A., Ré, C.: Flashattention: Fast and memory-efficient exact attention with io-awareness. *Advances in Neural Information Processing Systems* **35**, 16344–16359 (2022) 10
7. Deng, B., Genova, K., Yazdani, S., Bouaziz, S., Hinton, G., Tagliasacchi, A.: Cvxnet: Learnable convex decomposition. In: *Proceedings of the IEEE/CVF Conference on Computer Vision and Pattern Recognition (CVPR)* (June 2020) 1, 4
8. Erler, P., Guerrero, P., Ohrhallinger, S., Mitra, N.J., Wimmer, M.: Points2surf learning implicit surfaces from point clouds. In: *European conference on computer vision*. pp. 108–124. Springer (2020) 11
9. Gudkov, D.A.: The topology of real projective algebraic varieties. *Russian Mathematical Surveys* **29**(4), 1–79 (1974). <https://doi.org/https://doi.org/10.1070/RM1974v029n04ABEH001288> 3
10. Huang, J., Gojcic, Z., Atzmon, M., Litany, O., Fidler, S., Williams, F.: Neural kernel surface reconstruction. In: *Proceedings of the IEEE/CVF Conference on Computer Vision and Pattern Recognition*. pp. 4369–4379 (2023) 11
11. Itenberg, I., Viro, O.: Patchworking algebraic curves disproves the Ragsdale conjecture. *Mathematical Intelligencer* **18**(4) (1996) 2, 3, 4
12. Itenberg, I., Viro, O.: Asymptotically maximal real algebraic hypersurfaces of projective space. In: *Gökova Geometry/Topology conference*. pp. 91–105 (2006) 3, 4, 20, 21
13. Kazhdan, M., Hoppe, H.: Screened poisson surface reconstruction. *ACM Trans. Graph.* **32**(3) (Jul 2013). <https://doi.org/10.1145/2487228.2487237>, <https://doi.org/10.1145/2487228.2487237> 12
14. Khristoforov, M., Skopenkov, M., Smirnov, S.: A generalization of Cardy’s and Schramm’s formulae. *Communications in Mathematical Physics* **406**(5), 105 (2025) 6, 18
15. Koch, S., Matveev, A., Jiang, Z., Williams, F., Artemov, A., Burnaev, E., Alexa, M., Zorin, D., Panozzo, D.: Abc: A big cad model dataset for geometric deep learning. In: *The IEEE Conference on Computer Vision and Pattern Recognition (CVPR)* (June 2019) 11

16. Lipman, Y.: Phase transitions, distance functions, and implicit neural representations (2021), <https://arxiv.org/abs/2106.07689> 8
17. Lorensen, W.E., Cline, H.E.: Marching cubes: A high resolution 3d surface construction algorithm. *SIGGRAPH Comput. Graph.* **21**(4), 163–169 (Aug 1987). <https://doi.org/10.1145/37402.37422>, <https://doi.org/10.1145/37402.37422> 11
18. Maclagan, D., Sturmfels, B.: Introduction to tropical geometry, vol. 161. American Mathematical Soc. (2015) 3, 4
19. Maragos, P., Charisopoulos, V., Theodosis, E.: Tropical geometry and machine learning. *Proceedings of the IEEE* **109**(5), 728–755 (2021) 4
20. Maruani, N., Klovov, R., Ovsjanikov, M., Alliez, P., Desbrun, M.: Voromesh: Learning watertight surface meshes with voronoi diagrams. In: *Proceedings of the IEEE/CVF international conference on computer vision*. pp. 14565–14574 (2023) 12
21. Maruani, N., Ovsjanikov, M., Alliez, P., Desbrun, M.: Ponq: a neural qem-based mesh representation. In: *Proceedings of the IEEE/CVF conference on computer vision and pattern recognition*. pp. 3647–3657 (2024) 12
22. Miller, J., Sheffield, S., Werner, W.: CLE percolations. *Forum of Mathematics, Pi* **5**, e4 (2017). <https://doi.org/10.1017/fmp.2017.5> 18
23. Müller, T., Evans, A., Schied, C., Keller, A.: Instant neural graphics primitives with a multiresolution hash encoding. *ACM Trans. Graph.* **41**(4) (Jul 2022). <https://doi.org/10.1145/3528223.3530127>, <https://doi.org/10.1145/3528223.3530127> 1, 4
24. Pirahmad, O., Pottmann, H., Skopenkov, M.: Flexible polyhedral nets in isotropic geometry. *Beitr. Algebra Geom.* (2025), <https://doi.org/10.1007/s13366-025-00820-y> 6, 18
25. Ren, J., Zhang, B., Wu, B., Huang, J., Fan, L., Ovsjanikov, M., Wonka, P.: Intuitive and efficient roof modeling for reconstruction and synthesis. *ACM Trans. Graph.* **40**(6) (Dec 2021). <https://doi.org/10.1145/3478513.3480494>, <https://doi.org/10.1145/3478513.3480494> 11
26. Sellán, S., Ren, Y., Batty, C., Stein, O.: Reach for the arcs: Reconstructing surfaces from sdfs via tangent points. In: *SIGGRAPH 2024 Conference Papers* (2024) 11
27. Sellán, S., Batty, C., Stein, O.: Reach for the spheres: Tangency-aware surface reconstruction of sdfs (2023), <https://arxiv.org/abs/2308.09813> 11
28. Sharp, N., et al.: Polyscope (2019), www.polyscope.run 23
29. Siahkamari, A., Gangrade, A., Kulis, B., Saligrama, V.: Piecewise linear regression via a difference of convex functions. In: *International conference on machine learning*. pp. 8895–8904. PMLR (2020) 2, 9, 18
30. Sitzmann, V., Martel, J., Bergman, A., Lindell, D., Wetzstein, G.: Implicit neural representations with periodic activation functions. *Advances in neural information processing systems* **33**, 7462–7473 (2020) 3, 12
31. Sun, Y., Liu, Y., Niu, Y.S.: Understand the effectiveness of shortcuts through the lens of dca (2024), <https://arxiv.org/abs/2412.09853> 9
32. Takikawa, T., Litalien, J., Yin, K., Kreis, K., Loop, C., Nowrouzezahrai, D., Jacobson, A., McGuire, M., Fidler, S.: Neural geometric level of detail: Real-time rendering with implicit 3d shapes. In: *Proceedings of the IEEE/CVF Conference on Computer Vision and Pattern Recognition*. pp. 11358–11367 (2021) 1, 4
33. Tancik, M., Srinivasan, P., Mildenhall, B., Fridovich-Keil, S., Raghavan, N., Singhal, U., Ramamoorthi, R., Barron, J., Ng, R.: Fourier features let networks learn high frequency functions in low dimensional domains. *Advances in neural information processing systems* **33**, 7537–7547 (2020) 3

34. Tillet, P., Kung, H.T., Cox, D.: Triton: an intermediate language and compiler for tiled neural network computations. In: Proceedings of the 3rd ACM SIGPLAN International Workshop on Machine Learning and Programming Languages. p. 10–19. MAPL 2019, Association for Computing Machinery, New York, NY, USA (2019). <https://doi.org/10.1145/3315508.3329973>, <https://doi.org/10.1145/3315508.3329973> 10
35. Tulsiani, S., Su, H., Guibas, L.J., Efros, A.A., Malik, J.: Learning shape abstractions by assembling volumetric primitives. In: Proceedings of the IEEE Conference on Computer Vision and Pattern Recognition. pp. 2635–2643 (2017) 4
36. Viro, O.: Progress in the topology of real algebraic varieties over the last six years. *Russian Mathematical Surveys* **41**(3), 55–82 (1986). <https://doi.org/https://doi.org/10.1070/RM1986v041n03ABEH003317> 3, 4
37. Yariv, L., Puny, O., Gafni, O., Lipman, Y.: Mosaic-sdf for 3d generative models. In: Proceedings of the IEEE/CVF Conference on Computer Vision and Pattern Recognition. pp. 4630–4639 (2024) 4
38. Yuan, Q.: Hypersurfaces, 4-manifolds, and characteristic classes (2014), <https://qchu.wordpress.com/2014/06/16/hypersurfaces-4-manifolds-and-characteristic-classes/> 3, 21
39. Zhang, B., Tang, J., Niessner, M., Wonka, P.: 3DShape2VecSet: A 3d shape representation for neural fields and generative diffusion models. *ACM Transactions On Graphics (TOG)* **42**(4), 1–16 (2023) 4
40. Zhang, B., Wonka, P.: efunc: An efficient function representation without neural networks. *arXiv preprint arXiv:2505.21319* (2025) 4, 10
41. Zhang, L., Naitzat, G., Lim, L.H.: Tropical geometry of deep neural networks. In: International Conference on Machine Learning. pp. 5824–5832. PMLR (2018) 4
42. Zhou, Q., Jacobson, A.: Thing10k: A dataset of 10,000 3d-printing models. *arXiv preprint arXiv:1605.04797* (2016) 11